Available online at www.ifejost.org

IFE JOURNAL OF SCIENCE AND TECHNOLOGY

Vol 5. No. 1 (2021) 1–13

Spherical Spin-Coated Copper Tin Oxide Polycrystals from Inorganic Precursor: Synthesis, Surface Microstructural and Optical Characterization

O.E. Adewumi[1], E. Omotoso[1]*, R.A. Busari[1], S.A. Adewinbi[2], L.O. Animashaun[3], A.R. Lasisi[4] and B.A. Taleatu[1]

[1]Department of Physics and Engineering Physics, Obafemi Awolowo University, Ile-Ife, 220005, Nigeria
[2]Department of Physics, Osun State University Osogbo, Osun State, 232106, Nigeria
[3]Department of Physics, Fountain University Osogbo, Osun State, 230282, Nigeria
[4]Department of Physics, Federal College of Education Kontagora, 923101, Nigeria

* Corresponding author: omotoeze@gmail.com; eomotoso@oauife.edu.ng
Tel.: +234-806-445-2272.

Abstract

Thin film of copper doped tin oxide was deposited by spin coating technique. The Sn^{4+}, Cu^{2+} and O^{2-} were sourced from tin chloride, copper nitrate and potassium hydroxide. The films growth was achieved at a constant angular speed with variation in spun period. The samples were characterized by some surface techniques. Results from scanning electron microscopy (SEM) showed that the deposited films are amorphous with distinct and evenly distributed spherical particles across the substrate. Enhancement of films crystallinity and particles agglomeration was achieved by post-annealing. Elemental constituents of the film were evidently revealed. The optical behaviour of the films revealed the absorption edge at 593 and 709 nm, respectively. The obtained optical results are generally time dependent. The estimated average energy band gap of 2.83 eV suggested the appropriateness of deposited nanostructure as transparent contact electrodes in optoelectronic applications.

Keywords: Spin coating; Annealing; Crystallinity; Morphology; Energy band gap

Introduction

Energy consumption has increased because human activities depend on energy. It drives the world economy and sustains human development (Panwar *et al.*, 2011; Bajpai and Dash,

2012). Since the era of industrial revolution, fossil fuel was used in driving the economy, this resulted into climate change, environmental pollution and depletion of fossil fuel (Höök and Tang, 2013). Solar cells provide steady power at a cost-effective rate and it is essentially non-polluting. It is cheap and easily installed when compared to energy source such as hydroelectric, geothermal and nuclear power (Panwar *et al.*, 2011; Bajpai and Dash, 2012). Photovoltaic system is considered as a solution to problems caused by other sources of energy. It is a potential device that contributes in no small amount to the world energy by converting solar energy to electrical energy (Panwar *et al.*, 2011). Tin oxide has unique properties, such as good electrical conductivity, high optical transmittance, low resistivity, stability to heat treatment, mechanical hardness and non-toxicity (Salavati-Niasari *et al.*, 2010). SnO_2 thin films have great applications in chromic devices, flat panel display, gas sensors, invisible security circuits, liquid crystal displays, window layers, heat reflectors and solar cells (Watson, 1984; Minami, 2008). In an attempt to improve the physical, chemical properties and quality of tin oxide film, some metal ions can be added as impurities at low concentration. This brings about a modification in the catalytic activity, carrier concentration in the metal oxide matrix, crystallite size, etc. (Kumar and Rao, 2017). The applications of transparent conducting oxide in a device depend on their optical and electrical properties with electron work function, environmental stability, and compatibility with substrate (Du *et al.*, 2014). Thin films have been synthesized by various methods, such as electrodeposition, chemical vapour deposition, spray pyrolysis, molecular beam epitaxy, sputtering and spin coating (Hunt *et al.*, 1993; Sahu *et al.*, 2009). In this study, we report the growth of Cu-SnO_2 thin films from inorganic precursor using spin coating technique. The technique is employed due to its unique benefits such as film uniformity, low cost of equipment, simplicity to dope compounds and film reproduction (Mitzi, 2001).

Experimental Procedure

All chemical reagents used in this study are analytical grade (Sigma – Aldrich). They were used as received. The microscope glass slide substrates were cleaned by scrubbing thoroughly with cotton bud and soap solution, rinsed with running tap water and then ultrasonicated with distilled water, acetone and methanol at 40°C for ten minutes each. They were dried briefly in open furnace. An Osilla spin coater (E440) from Osilla Limited, Sheffield, UK was used as growth device. Each coating took between 10 and 20 sec.

Preparation of precursor and sample deposition

Solution precursors were prepared from commonly sourced chemical reagents. 0.5 M of $SnCl_2$ solution was prepared by adding 12.08 g of $SnCl_2.2H_2O$ salt in 100 ml of methanol. Also, 0.5 M of KOH was prepared by mixing 2.0 g of potassium hydroxide pellet in 100 ml of methanol. In addition, 0.05 M of $Cu(NO_3)_2$was prepared by dissolving 1.21 g of $Cu(NO_3)_2.5H_2O$ in 100 ml of methanol. At room temperature, solutions prepared were kept in different flasks for twenty-four hours to enhance thorough dissolution. The spin coated

precursor was made by mixing 20 ml each of $SnCl_2$ and KOH and 5 ml of $Cu(NO_3)_2$ together in a beaker. The resulting solution was properly stirred for five hours at room temperature to increase the viscosity of the prepared precursor. The precursor was then spin coated on the substrate at 3500 rpm at varied deposition time, for two cycles. Sample AA1 was obtained by coating the substrate for 5 sec per cycle and sample AA2 was obtained by coating for 10 sec per cycle. Total deposition time for samples AA1 and AA2 at 3500 rpm were 10 and 20 seconds, respectively.

Sample characterization

Samples were dried at 100°C for 5 minutes in an open furnace after deposition to remove residual organic solvent and were later annealed at 300°C for 30 minutes to improve the crystallinity of the nanostructure. Surface morphology and chemical composition were studied using Zeiss ultra plus field emission scanning electron microscopy (FE-SEM) attached with energy dispersive X-ray spectroscopy (EDX) facility. A XPERT-PRO X-ray diffractometer (PANalytical BV, Netherlands) with reflection geometry ranging from 2θ values between 10 to 90° with a step size of 0.01°, operating with a Co K_α radiation source (λ = 0.178901 nm) at 50 kV and 30 mA was used to obtain the X-ray diffraction patterns. Optical transmittance and absorption of deposited films were studied across the visible spectrum region by a double beam UV/VIS spectrophotometer.

Results and Discussion

Crystal structure and orientation

Figure 1 shows the XRD pattern of Cu-SnO_2 thin film, not many diffraction peaks are identified. This implies that deposition layers are poorly crystalline. However, an intense peak observed at plane (101) still indicates that the samples are poorly amorphous. The suppression of this peak when the deposition took longer time could suggest that the film's surface was overlapped with amorphous substances from the coating gel. Thus, the longer time of the spin coating does not necessarily lead to production of more durable film. Across all the diffraction angles, peaks due to Cu^{2+} were not detected. This could be attributed to limitations from the used XRD machine, most important its power ratings might not be enough to identify the Cu particle (Islam *et al.*, 1996; Choudhury *et al.*, 2015; Benzitouni *et al.*, 2016). The prominent peak is along the plane (101) which is characteristic of the deposited samples **(**Cu-SnO_2) film with tetragonal crystal

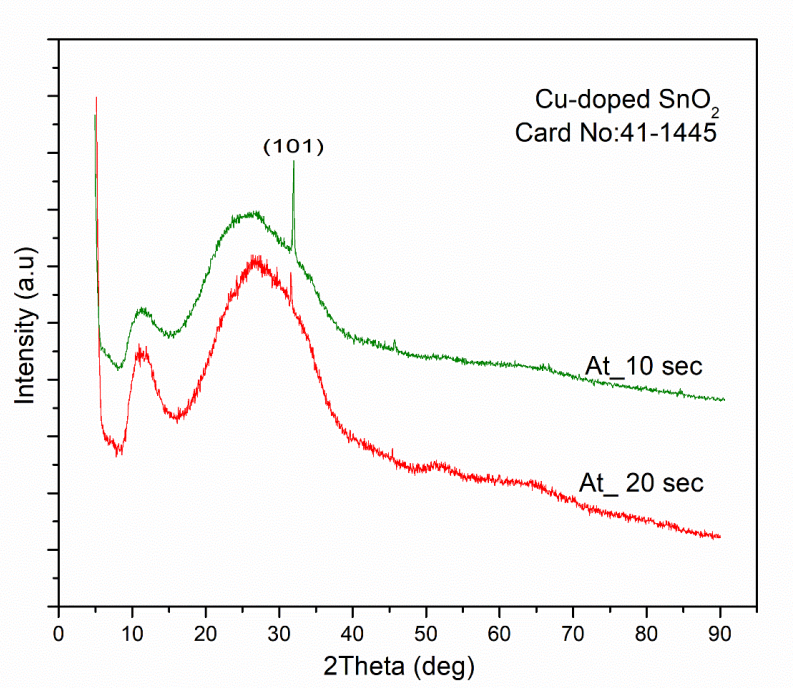

Figure 1: XRD patterns of Cu-SnO_2 thin film at different deposition times

structure and are consistent with JCPDS card no: 41-1445. Interplanar spacing, d, of the deposited thin film was determined by Equation 1

$$\frac{1}{d^2} = \frac{h^2+k^2}{a^2} + \frac{l^2}{c^2} \qquad (1)$$

where a and c are lattice constants, and h, k, l are Miller indices. Also, the average size of the crystallites, D for Cu-SnO_2 thin film was determined by Williamson Hall's modified Debye Scherrer's formula in Equation 2 (Adewinbi *et al.*, 2020):

$$\beta = \frac{k\lambda}{D\cos\theta} + 4\varepsilon\tan\theta \qquad (2)$$

where β is the full width at half maximum (FWHM) of the most prominent peaks measured in radians, the constant k is 0.94, λ is the wavelength of the incident X-ray, θ is Bragg's diffraction angle and ε is the residual lattice strain of the thin films. The average crystal sizes and lattice strains of the samples were determined from the intercept and slope of the plot of $\beta\cos\theta$ versus $\sin\theta$ (Bagheri *et al.*, 2013).

Dislocation density, was determined using the Equation 3 (Busari *et al.*, 2020):

$$\delta = \frac{1}{d^2} \quad (3)$$

where d represents the interplanar spacing.

Table 1 shows the value ε, D, δ, a, b and FWHM of the materials. From the table, it is observed that as growth time increases, the interplanar spacing d, crystallite size D, dislocation density δ and lattice strain ε of the material increase. Similar observation has been reported in the literature (Kaiser, 2002).

Table 1: Calculated data from XRD pattern with a and b as lattice constants

Sample	2θ	Hkl	FWHM	Lattice Constant		d (Å)	D (nm)	δ (nm)^2	ε
				a	b				
AA1	30.76	101	0.1417	4.110	4.061	2.91	101.10	9.78	0.034
AA2	30.53	101	0.1882	4.140	4.139	2.93	86.55	13.35	0.046

3.2. Surface morphology

SEM micrographs of Cu-SnO_2 thin films are shown in Figure 2(a and b). Distinct spherical particles evenly distributed across the substrate were evidently observed, some drifts are fused together to form giant polycrystals. Some overgrown particles were observed. Also, the image analysis showed the particle size of sample AA1 in nanometer scale (~17 nm) but at higher deposition time, the nanoparticles agglomerate to form densely

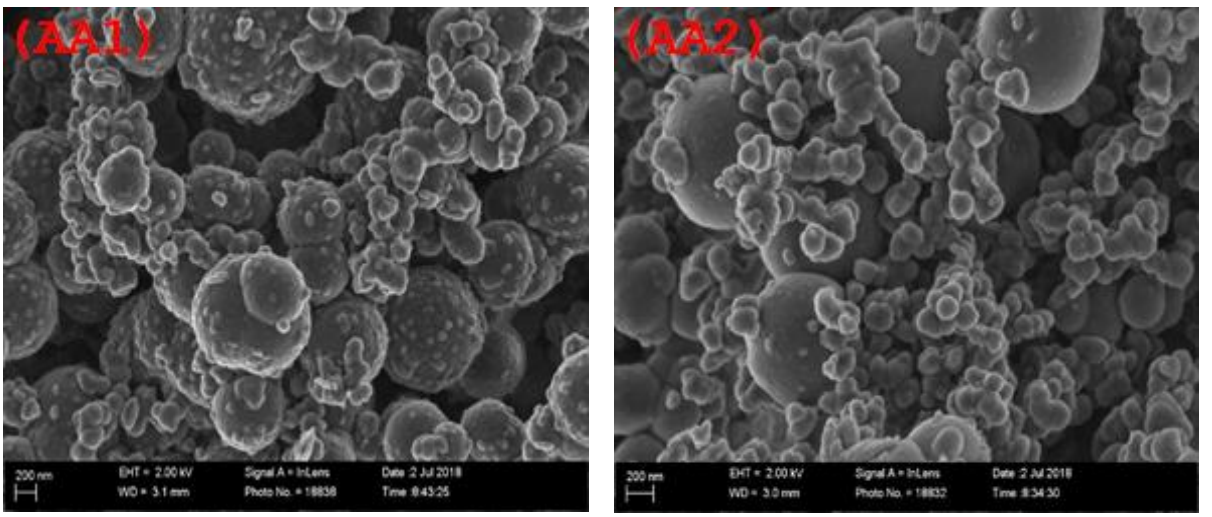

Fig. 2. Surface morphology of theCu-SnO_2 thin films at different deposition time for (a) AA1 and (b) AA2

packed particles and therefore, enhance particle sizes in samples AA2 (~30nm). However, film crystallinity was enhanced by post-deposition annealing. Cu ions (dopant) are well integrated into the lattice of the host nanostructure (SnO_2). This could be a reason for an absence of cracks in the deposited film (Han *et al.*, 2011).

Films composition

Figure 3 showed the spectra obtained when deposited samples were studied quantitatively by Energy Dispersive Spectroscopy (EDS). The presence of Sn, O and some traces of copper was revealed by the spectra obtained. Also, other elements in the spectra are attributable to the substrate. Table 2 presents the percentage atomic weight of the grown nanostructure samples.

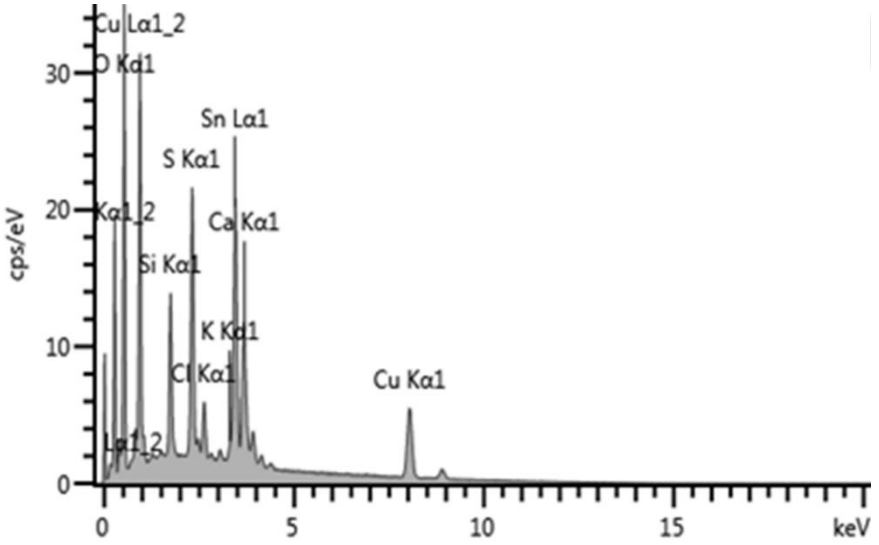

Fig. 3. EDS elemental analysis of deposited Cu-SnO_2 thin film

Table 2: EDS elemental analysis deposited Cu-SnO_2 thin film

Element	C	O	Si	S	Cl	K	Ca	Cu	Sn	Total
wt %	19.38	21.97	2.95	5.79	1.45	0.50	0.62	20.83	26.51	100.00
Atomic %	41.46	35.27	2.70	4.94	1.05	0.33	0.40	8.42	5.74	100.00

3.4 Rutherford Backscattering Spectroscopy (RBS)

The elemental composition and film thickness were further studied by Rutherford Backscattering Spectroscopy (RBS). The result confirmed the presence of copper, tin and oxygen in the samples (see Figure 4).

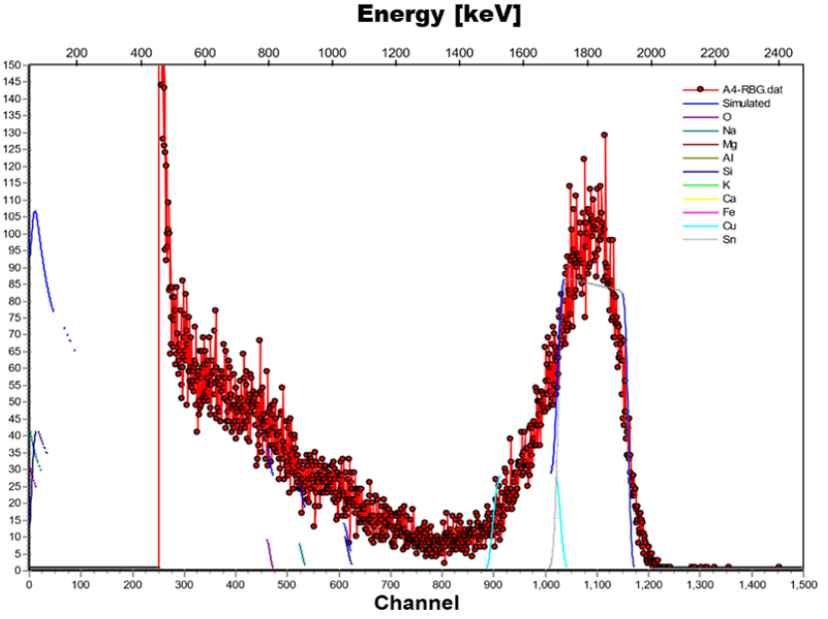

Figure 4: RBS spectrum of Cu-SnO_2 thin film

Table 3 reveals the percentage composition of the deposited thin film. The obtained result from the RBS revealed that the film's stoichiometry is $Cu_{0.2}Sn_{0.8}O_{2.2}$. Applying the obtained data from RBS studies in the equation 4, film thickness was estimated approximately as 210 nm.

$$\textbf{Thickness} = \frac{\textit{Atoms per unit area}}{\textbf{Atomic density}} \tag{4}$$

Table 3: Percentage composition of deposited Cu-SnO_2 film

Element	% Composition	Ratio
Cu	6.12	0.2
Sn	29.52	0.8
O	64.32	2.2

Optical characterization

Films optical properties were studied across UV/VIS range. The results are shown in Figure 5(a – d). Deterioration in absorbance is observed from visible to infrared region with a red shift in spectra depicted in Figure 5a.

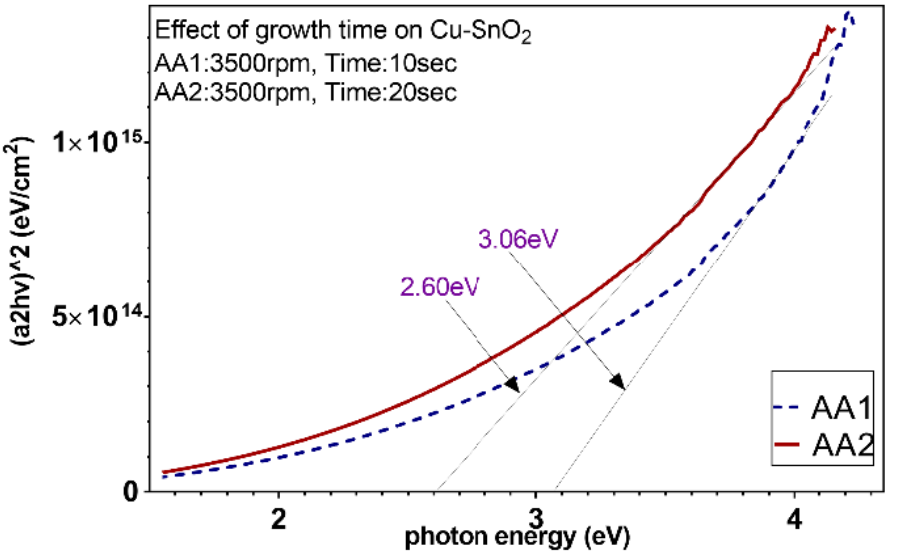

Figure 5a: UV-visible absorption coefficient spectrum of deposited Cu-SnO_2 thin film. The absorption edges AAI and AA2 are 593 and 709 nm respectively

At longer deposition, sample demonstrated better absorbance. Film thickness could be responsible for this manifestation. In addition, there is a change in photon energy at the optical absorption edge, as a result of excitation of electrons from lower energy level to higher energy level (Zhang *et al.*, 2013; Murata *et al.*, 2015). Transparent conducting oxides (TCO) semiconductors with such property are applied as buffer layer in inorganic photovoltaic devices (Elias *et al.*, 2007). Figure 5b, shows clearly that the surface quality and film homogeneity were enhanced. It was also noted that film transmittance in the visible region was higher, because of low reflectivity and low absorption. Cu-SnO_2 film synthesized at shorter time transmits better in the visible region. The absorption coefficient (α) could be calculated by Equation 5, (Busari *et al.*, 2019);

$$\alpha = 2.303\frac{A}{t} \quad (5)$$

where *A* and *t* are absorbance and film thickness.

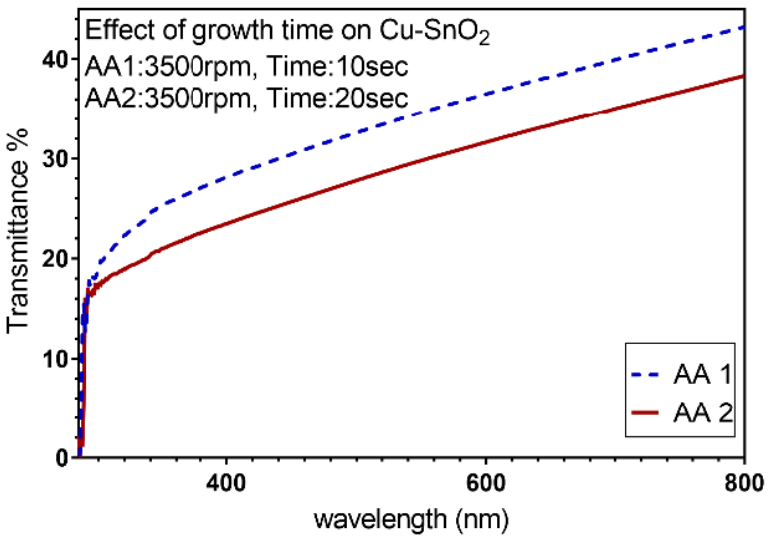

Figure 5b: UV-visible transmittance spectrum of deposited Cu-SnO_2 thin film

.

In Figure 5c, Absorption data were applied to generate Tauc's plots, and the energy band gaps were estimated based on the Equation 6.

$$\alpha h\nu = B\left(h\nu - E_g\right)^{\frac{n}{2}} \tag{6}$$

where direct and indirect band gaps are represented by n =1 and 4 respectively. α denotes the absorption coefficient, B represents an empirical constant, $h\nu$ is the incident photon energy and E_g denotes the energy band gap. By extrapolating the linear portion of $(\alpha h\nu)^2$ versus $h\nu$, at $(\alpha h\nu)^2 = 0$, the energy band gaps of the samples were estimated (Ferhat *et al.*, 2009). Spectrum from sample AA2 with longer deposition time has lower energy band gap than AA1 produced at shorter deposition time. This implies that optical band gap decreases with increase in deposition time. The lower energy band gap in sample AA2 is due to growth of grains and addition of more donor energy level by impurities, into the host semiconductor. This brings about a shift in Fermi level closer to band edges (Ferhat *et al.*, 2009; Li *et al.*, 2003). Increasing the deposition time of sample, results into an increase in the density of states generated by dopant. This density of state produces a band of states below the conduction bands leading to a decrease in energy band gap. The optical energy of a semiconductor defines the threshold of photon absorption. It also exemplifies a fundamental property describing the optical and electronic property of a semiconductor.

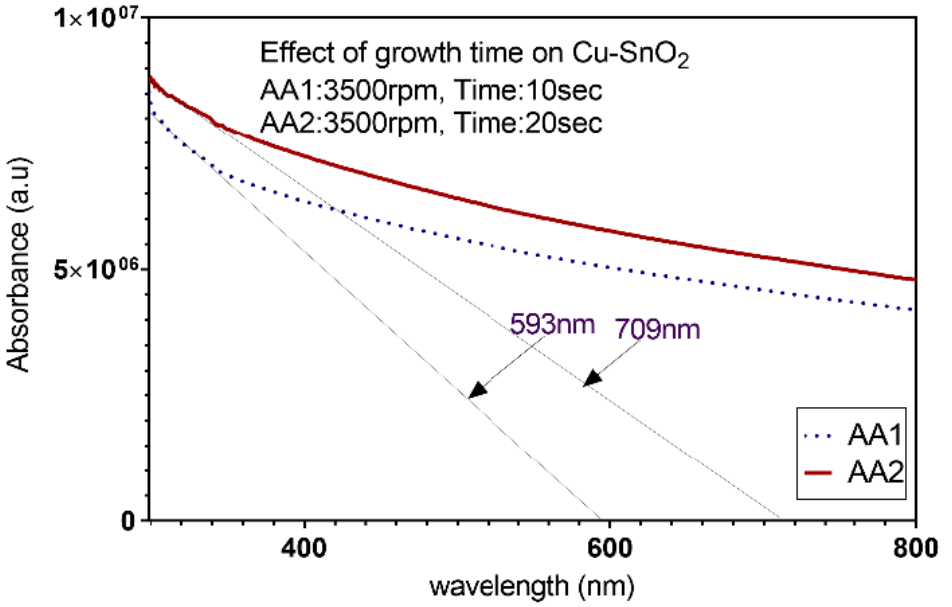

Figure 5c: Tauc's plot for estimation of energy band gap of Cu-SnO_2 thin film. The energy band gaps are 2.60 eV and 3.06 eV, respectively.

Figure 5d depicts a plot of skin depth against photon energy. The spectra obtained evidently revealed that skin depth decreases with photon energy. Sample AA2 has lower skin depth than sample AA1.The trend of spectra is similar to those obtained from the transmittance plot.

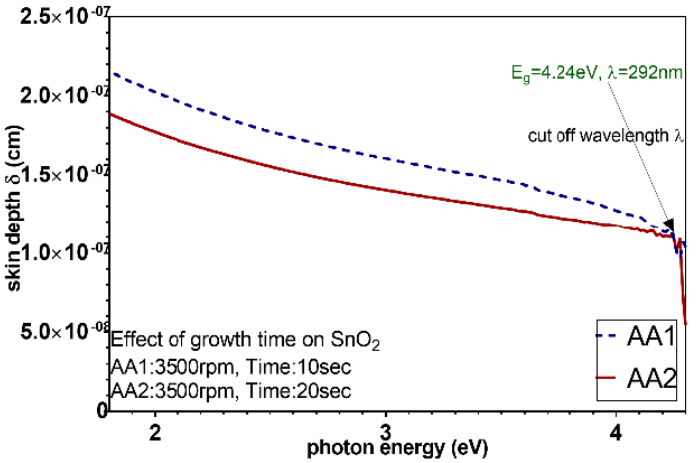

Figure 5d: Skin depth plot for deposited Cu-SnO_2 thin film.

Conclusions

In this study, Cu-SnO_2 thin film was successfully deposited on sodalime glass slides by spin coating technique. XRD pattern of the deposited film was not characterized with multiple peaks suggesting that the film is poorly polycrystalline. The preferred orientation of the film along the plane (101) revealed that the deposited film exhibits tetragonal crystal structure. Morphological studies revealed uniform and well distributed films across the surface of the substrate. It is observed from the micrograph that the grain agglomeration is a function of deposition time. The film crystallinity was enhanced by post-deposition annealing. EDS spectra showed peaks corresponding to elements in the film and the substrate. The optical absorption edges were estimated between 593 and 709 nm for the samples, respectively. The obtained estimated direct energy band gap suggested that the deposited film can function as good transparent contact electrode in optoelectronic devices.

Acknowledgements

This work is supported by The World Academy of Science and the Abdus Salam International Centre for Theoretical Physics with Research Grant number 15-049 RG/PHYS/AF/AC_I-FR3240287081. We acknowledge the efforts of Mr. M.A. Ramon of Department of Chemistry and staff of Materials Science laboratory in the Department of Physics and Engineering Physics of Obafemi Awolowo University Ile-Ife, Nigeria.

References

Adewinbi, S. A., Taleatu, B. A., Busari, R. A., Adewumi, O. E., Omotoso, E., Oyedotun, K. O., and Manyala, N. (2020). Preparation and Surface Characterization of Nanostructured MoO_3/Co_xO_y and V_2O_5/C_xO_y Interfacial Layers as Transparent Oxide Structures for Photoabsorption. *Journal of Electronic Materials*, 49(6) 1-12.

Bagheri, S., Chandrappa, K. G., and Hamid, S. A. (2013). "Facile synthesis of nano-sized ZnO by direct precipitation method". *Der PharmaChemica*, 5(3): 265-270.

Bajpai, P., and Dash, V. (2012). Hybrid renewable energy systems for power generation in stand-alone applications: A review. *Renewable and Sustainable Energy Reviews*, *16*(5), 2926-2939.

Benzitouni, S., Zaabat, M., Khial, A., Rechem, D., Benaboud, A., Bouras, D., and Coste, R. (2016). "High sensitivity of porous Cu-doped SnO_2 thin films to methanol". *Adv. Nanoparticles*, 5(2): 140.

Busari, R. A., Taleatu, B. A., Adewinbi, S. A., Adewumi, O. E., Fasasi, A. Y.(2019). Surface Characterisation of Spin Coated Quaternary Chalcogenide CZT(S, O) Thin Film for Optoelectronic Applications. *Journal of Photonic Materials and Technology*, 5(2), 38-45.

Busari, R. A., Taleatu, B. A., Adewinbi, S. A., Adewumi, O. E., Omotoso, E., Oyedotun, K. O., &Fasasi, A. Y. (2020). Synthesis and surface characterization of electrodeposited

quaternary chalcogenide $Cu_2Zn_xSn_yS_{1+x+2y}$ thin film as transparent contact electrode. *Bulletin of Materials Science*, *43*(1), 1-9.

Choudhury, B., Choudhury, A., and Borah, D. (2015). "Interplay of dopants and defects in making Cu doped TiO_2 nanoparticle a ferromagnetic semiconductor". *Journal of Alloys and Compounds*, 646: 692-698.

Du, J., Pei, S., Ma, L., and Cheng, H. M. (2014). 25th anniversary article: carbon nanotube-and graphene-based transparent conductive films for optoelectronic devices. *Advanced materials*, *26*(13), 1958-1991.

Elias, J., Tena-Zaera, R., and Lévy-Clément, C. (2007). Electrodeposition of ZnO nanowires with controlled dimensions for photovoltaic applications: Role of buffer layer. *Thin Solid Films*, *515*(24), 8553-8557.

Ferhat, M., Zaoui, A., and Ahuja, R. (2009). Magnetism and band gap narrowing in Cu-doped ZnO. *Applied Physics Letters*, *94*(14), 142502.

Han, C., Pelaez, M., Likodimos, V., Kontos, A. G., Falaras, P., O'Shea, K., and Dionysiou, D. D. (2011). Innovative visible light-activated sulfur doped TiO2 films for water treatment. *Applied Catalysis B: Environmental*, *107*(1-2), 77-87.

Höök, M., and Tang, X. (2013). Depletion of fossil fuels and anthropogenic climate change—A review. *Energy policy*, *52*, 797-809.

Hunt, A. T., Carter, W. B., and Cochran Jr, J. K. (1993). Combustion chemical vapor deposition: A novel thin-film deposition technique. *Applied Physics Letters*, *63*(2), 266-268.

Islam, M. N., Ghosh, T. B., Chopra, K. L., and Acharya, H. N. (1996). XPS and X-ray diffraction studies of aluminum-doped zinc oxide transparent conducting films. *Thin solid films*, *280*(1-2), 20-25.

Kaiser, N. (2002). Review of the fundamentals of thin-film growth. *Applied optics*, *41*(16), 3053-3060.

Kumar, S. G., and Rao, K. K. (2017). Comparison of modification strategies towards enhanced charge carrier separation and photocatalytic degradation activity of metal oxide semiconductors (TiO2, WO3 and ZnO). *Applied Surface Science*, *391*, 124-148.

Li, W., Wang, Y., Lin, H., Ismat Shah, S., Huang, C. P., Doren, D. J., ... and Barteau, M. A. (2003). Band gap tailoring of Nd 3+-doped TiO 2 nanoparticles. *Applied Physics Letters*, *83*(20), 4143-4145.

Minami, T. (2008). Substitution of transparent conducting oxide thin films for indium tin oxide transparent electrode applications. *Thin solid films*, *516*(7), 1314-1321.

Mitzi, D. B. (2001). Thin-film deposition of organic− inorganic hybrid materials. *Chemistry of Materials*, *13*(10), 3283-3298.

Murata, M., Chantana, J., Ashida, N., Hironiwa, D., and Minemoto, T. (2015). Influence of conduction band minimum difference between transparent conductive oxide and absorber on photovoltaic performance of thin-film solar cell. *Japanese Journal of Applied Physics*, *54*(3), 032301.

Panwar, N. L., Kaushik, S. C., and Kothari, S. (2011). Role of renewable energy sources in environmental protection: A review. *Renewable and sustainable energy reviews*, *15*(3), 1513-1524.

Sahu, N., Parija, B., and Panigrahi, S. (2009). Fundamental understanding and modeling of spin coating process: A review. *Indian Journal of Physics*, *83*(4), 493-502.

Salavati-Niasari, M., Mir, N., and Davar, F. (2010). Synthesis, characterization and optical properties of tin oxide nanoclusters prepared from a novel precursor via thermal decomposition route. *Inorganica Chimica Acta*, *363*(8), 1719-1726.

Watson, J. (1984). The tin oxide gas sensor and its applications. *Sensors and Actuators*, *5*(1), 29-42.

Zhang, S., Li, W., Yao, L., Pan, Y., Shen, F., Xiao, R. and Ma, Y. (2013). "Enhanced proportion of radiativeexcitons in non-doped electro-fluorescence generated from an imidazole derivative with an orthogonal donor–acceptor structure". *Chem. Comm.*, 49(96): 11302-11304.